PHYSICAL REVIEW D **79,** 124018 (2009)

Quasiequilibrium states of black hole-neutron star binaries in the moving-puncture framework

Koutarou Kyutoku and Masaru Shibata
Yukawa Institute for Theoretical Physics, Kyoto University, Kyoto, 606-8502, Japan

Keisuke Taniguchi
Department of Physics, University of Wisconsin-Milwaukee, P.O. Box 413, Milwaukee, Wisconsin 53201, USA
(Received 18 March 2009; published 12 June 2009)

General relativistic quasiequilibrium states of black hole-neutron star binaries are computed in the moving-puncture framework. We propose three conditions for determining the quasiequilibrium states and compare the numerical results with those obtained in the excision framework. We find that the results obtained in the moving-puncture framework agree with those in the excision framework and with those in the third post-Newtonian approximation for the cases that (i) the mass ratio of the binary is close to unity irrespective of the orbital separation, and (ii) the orbital separation is large enough ($m_0\Omega \lesssim 0.02$, where m_0 and Ω are the total mass and the orbital angular velocity, respectively) irrespective of the mass ratio. For $m_0\Omega \gtrsim 0.03$, both of the results in the moving-puncture and excision frameworks deviate, more or less, from those in the third post-Newtonian approximation. Thus the numerical results do not provide a quasicircular state, rather they seem to have a non-negligible eccentricity of order 0.01–0.1. We show by numerical simulation that a method in the moving-puncture framework can provide approximately quasicircular states in which the eccentricity is by a factor of ~ 2 smaller than those in quasiequilibrium given by other approaches.

DOI: 10.1103/PhysRevD.79.124018 PACS numbers: 04.25.D−, 04.30.−w, 04.40.Dg

I. INTRODUCTION

Ground-based laser interferometric gravitational-wave detectors such as LIGO [1], VIRGO [2], GEO600 [3], and TAMA300 [4] are now in operation, and advanced detectors such as advanced LIGO will be in operation in the next decade and are expected to detect gravitational waves. Among many other sources, coalescing binary compact objects such as neutron star-neutron star and black hole-neutron star (hereafter NS-NS and BH-NS, respectively) binaries are the most promising sources [5–7]. This has been motivating theoretical studies of gravitational waves from the inspiral and merger of the binary compact objects.

In the past two decades, a number of short-hard γ-ray bursts has been observed by the γ-ray and x-ray satellites [8,9]. However, the progenitors of these bursts are still highly uncertain. One of the plausible models of the central engine is the merger of NS-NS and/or BH-NS binaries [10,11]. This scenario is based on the idea that a system consisting of a rotating BH and hot, massive accretion-disk is formed as a consequence of the merger, and subsequently, they emit huge amount of γ-rays and x-rays in a short time scale. To theoretically explore this possibility (more specifically, to clarify the formation process of the BH-disk system), general relativistic study for the merger of NS-NS and BH-NS binaries is probably the unique approach. This issue has been also motivating numerical studies for the merger of NS-NS and BH-NS binaries.

In the past decade, substantial effort has been paid in the community of numerical relativity for clarifying the inspiral and merger processes of binary compact objects. In particular, a wide variety of simulations have been performed for the merger of NS-NS binaries [12–21] and black hole-black hole (hereafter BH-BH) binaries [22–50]. In the past two years, a method for computing quasiequilibrium states of BH-NS binaries has been developed [51–55], and also, numerical simulations for the merger of BH-NS binaries have been done [56–61]. However, these researches are still in early stage; e.g., most of the simulations have been performed only for a short time scale, and for such simulations, the inspiral and subsequent merger phases are not likely to be computed very accurately (but see [62,63]). Also, it is not clear whether the computed quasiequilibrium states are really quasicircular; i.e., it is not clear whether the eccentricity is sufficiently small. Numerical simulations are performed employing the quasiequilibrium states as the initial condition. If the quasiequilibrium state is not in a quasicircular orbit, the results of the numerical simulation are not realistic. The purpose of this paper is (i) to present an improved study for the quasiequilibrium states and (ii) to compare several quasiequilibrium states obtained so far. In an accompany paper [63], we also present the latest accurate numerical results for the inspiral and merger of BH-NS binaries.

To compute a quasiequilibrium state of BH-NS binaries, we have to employ an appropriate method by which the singular behavior of the BH is avoided. In most of the previous studies [51–55], the quasiequilibrium state is computed in the so-called excision framework, in which a spherical region inside an apparent horizon is excised and basic equations are solved imposing plausible boundary

conditions at the excised two-sphere. In this paper, we employ the so-called moving-puncture approach (see Sec. II A), which is an alternative of the excision approach [56,57]. In this approach, we do not have to excise any region around the BH horizon nor impose boundary conditions around the BH, as shown in Ref. [64]. Indeed, this has been proven to be quite useful for computing a quasiequilibrium state [65] and also for simulating binary BHs (e.g., [24,28]).

Another possible merit in the moving-puncture approach is that there is a flexibility for computing a quasiequilibrium state. In the excision method, one imposes the boundary conditions at the excised two-sphere and at spatial infinity. The boundary conditions at the excised surface are usually determined by requiring that the two-sphere should be the Killing horizon at least approximately. As a result, a quasiequilibrium state is completely determined with no ambiguity, although it is not clear whether the obtained quasiequilibrium is really a quasicircular state [66]. By contrast, any boundary condition does not have to be imposed around the BH in the moving-puncture approach. Because of this, we have a remaining degree of freedom for defining a quasiequilibrium state. Specifically, we do not have any natural, physical condition for determining the center of mass of the system in this method. However, this degree of freedom can be used to obtain a favorable, quasiequilibrium state. As we illustrate in Sec. III, quasiequilibrium states obtained in the excision method are not quasicircular in general: Namely, the eccentricity is not zero (see also Ref. [66]). In the moving-puncture approach, the remaining degree of freedom can be used to reduce the eccentricity, and it may be possible to obtain a quasiequilibrium state in which the eccentricity is smaller than that obtained by the excision method.

This paper is organized as follows: In Sec. II, we first review the basic equations for computing quasiequilibrium states in the moving-puncture approach. Then, we describe three methods for determining the center of mass in the moving-puncture approach. The numerical methods for solving a quasiequilibrium state are described in Sec. III. We present our numerical results and compare those with other results in Sec. IV. In Sec. IV C, we present results of numerical simulation of the inspiral and merger of BH-NS binaries for a particular model: We adopt two initial data obtained in the moving-puncture approach, and compare the numerical results. We then demonstrate that one of the moving-puncture approach is superior for the initial condition because the eccentricity is smaller than those obtain in other methods. Section V is devoted to a summary. Throughout this paper, we adopt the geometrical units in which $G = c = 1$, where G and c are the gravitational constant and the speed of light. Latin and Greek indices denote spatial and spacetime components, respectively.

II. FORMULATION

In this section, we first review the basic equations for computing a BH-NS binary in quasiequilibrium, and then describe the quantities used in the analysis and the methods for defining the quasiequilibrium state in the moving-puncture approach.

A. Field equations in the moving-puncture framework

To derive a quasiequilibrium state of BH-NS binaries as a solution of the initial value problem of general relativity, we employ a mixture of the conformal thin-sandwich decomposition [67] and conformal transverse-traceless decomposition of the Einstein equations. Following the previous works, we assume that the trace part of the extrinsic curvature ($K = \mathrm{tr}(K_{ij})$) is zero and the three-metric (γ_{ij}) is conformally flat [68]: $\gamma_{ij} = \psi^4 f_{ij}$, where ψ is the conformal factor and f_{ij} is the flat metric.

We define a tracefree, weighted extrinsic curvature as

$$\hat{A}^{ij} = \psi^{10} K^{ij}. \tag{1}$$

Because we assume that the three-metric is conformally flat, this quantity is written by

$$\hat{A}^{ij} = \frac{\psi^6}{2\alpha}\left(\hat{\nabla}^i \beta^j + \hat{\nabla}^j \beta^i - \frac{2}{3} f^{ij} \hat{\nabla}_k \beta^k\right), \tag{2}$$

where α is the lapse function, β^k the shift vector, and $\hat{\nabla}_i$ the covariant derivative with respect to f_{ij}. Note that adding a rotational shift vector,

$$\beta^i_{\mathrm{rot}} = (\boldsymbol{\Omega} \times \mathbf{R})^i, \tag{3}$$

does not change $\hat{A}^{ij}$ in the conformal flatness formalism. Here, Ω is the angular velocity vector of the binary and R is the coordinate vector from the center of mass of the binary. Thus, computation may be performed in any rotational frame using the same equations, by simply changing the boundary conditions.

In the present formalism, the basic equations are derived from the Hamiltonian constraint, momentum constraint, and the maximal slicing condition ($\partial_t K = 0$) [69] as

$$\Delta\psi = -2\pi\psi^5 \rho_H - \tfrac{1}{8}\psi^{-7}\hat{A}_{ij}\hat{A}^{ij}, \tag{4}$$

$$\Delta\beta^i + \tfrac{1}{3}\hat{\nabla}^i\hat{\nabla}_j\beta^j = 16\pi\alpha\psi^4 j^i + 2\hat{A}^{ij}\hat{\nabla}_j(\alpha\psi^{-6}), \tag{5}$$

$$\Delta\Phi = 2\pi\Phi\psi^4(\rho_H + 2S^k_k) + \tfrac{7}{8}\Phi\psi^{-8}\hat{A}_{ij}\hat{A}^{ij}, \tag{6}$$

where $\Delta = f^{ij}\hat{\nabla}_i\hat{\nabla}_j$, $\Phi \equiv \alpha\psi$, and

$$\rho_H = T^{\mu\nu} n_\mu n_\nu, \tag{7}$$

$$j^i = -T^{\mu\nu} n_\mu \gamma^i_\nu, \tag{8}$$

$$S_{ij} = T^{\mu\nu}\gamma_{i\mu}\gamma_{j\mu}. \tag{9}$$

Here, n^μ is the timelike hypersurface normal, $\hat{A}_{ij} = f_{ik}f_{jl}\hat{A}^{kl}$, and $T^{\mu\nu}$ the stress-energy tensor.

For computing a quasiequilibrium state of a system containing BHs, we have to appropriately treat singular behaviors of the BHs because divergent quantities cannot be handled in numerical computation. Most of the previous works for computing quasiequilibrium states of BH-NS binaries [51–55] have been done with an "excision approach," i.e., excising the region inside two-sphere of apparent horizon from the computational domain with appropriate boundary conditions at the excision surface. On the other hand, a "puncture" method [64] was proposed by Brandt and Brügmann to describe multiple BHs with arbitrary linear momenta and spin angular momenta, and a "moving-puncture approach" [24,28] was revealed to be quite useful in dynamical simulations. In this paper, we employ the moving-puncture approach, which is developed by Shibata and Uryū [56,57] for the case of BH-NS binaries. In the puncture or moving-puncture framework we decompose the metric quantities into a singular part, which is written analytically and denotes contribution from a BH, and a regular part, which is obtained by numerically solving the basic equations. Assuming that the puncture is located at $\boldsymbol{r}_{\rm P} = x^k_{\rm P}$, we set ψ and Φ as

$$\psi = 1 + \frac{M_{\rm P}}{2r_{\rm BH}} + \phi, \tag{10}$$

$$\Phi = 1 - \frac{M_\Phi}{r_{\rm BH}} + \eta, \tag{11}$$

where $M_{\rm P}$ and M_Φ are positive constants of mass dimension, and $r_{\rm BH} = |x^k - x^k_{\rm P}|$ is a coordinate distance from the puncture. $M_{\rm P}$ is an arbitrarily chosen parameter called the puncture mass, whereas M_Φ is determined by the condition that Arnowitt-Deser-Misner (ADM) mass (M_0), and Komar mass agree (this condition should hold when the spacetime is stationary and asymptotically flat [70,71]), i.e.,

$$\oint_{r\to\infty} \partial_i \Phi dS^i = -\oint_{r\to\infty} \partial_i \psi dS^i = 2\pi M_0. \tag{12}$$

Also, we decompose $\hat{A}_{ij}$ into singular and regular parts as

$$\hat{A}_{ij} = \hat{\nabla}_i W_j + \hat{\nabla}_j W_i - \tfrac{2}{3} f_{ij}\hat{\nabla}_k W^k + K^{\rm P}_{ij}, \tag{13}$$

where $K^{\rm P}_{ij}$ is the singular part, which denotes a weighted extrinsic curvature associated with the linear momentum of the BH written by

$$K^{\rm P}_{ij} = \frac{3}{2r^2_{\rm BH}}[l_i P^{\rm BH}_j + l_j P^{\rm BH}_i - (f_{ij} - l_i l_j) l^k P^{\rm BH}_k], \tag{14}$$

and $l^k = x^k_{\rm BH}/r_{\rm BH}$. W_i denotes an auxiliary three-dimensional function and $W^i = f^{ij}W_j$. Because the total linear momentum of the system should vanish, the linear momentum of the BH, $P^{\rm BH}_i$, is related to that of the companion NS as

$$P^{\rm BH}_i = -\int j_i \psi^6 dV, \tag{15}$$

where the right-hand side denotes the (minus) linear momentum of the NS.

Field equations that we have to solve are summarized as follows:

$$\Delta\phi = -2\pi\psi^5\rho_H - \tfrac{1}{8}\psi^{-7}\hat{A}_{ij}\hat{A}^{ij}, \tag{16}$$

$$\Delta\beta^i + \tfrac{1}{3}\hat{\nabla}^i\hat{\nabla}_j\beta^j = 16\pi\Phi\psi^3 j^i + 2\hat{A}^{ij}\hat{\nabla}_j(\Phi\psi^{-7}), \tag{17}$$

$$\Delta\eta = 2\pi\Phi\psi^4(\rho_H + 2S^k_k) + \tfrac{7}{8}\Phi\psi^{-8}\hat{A}_{ij}\hat{A}^{ij}, \tag{18}$$

$$\Delta W_i + \tfrac{1}{3}\hat{\nabla}_i\hat{\nabla}_j W^j = 8\pi\psi^6 j_i. \tag{19}$$

We note that $\hat{A}_{ij}$ is obtained by Eq. (13), not by Eq. (2), because $\hat{A}^{ij}$ is not straightforwardly defined for $\alpha = 0$ when we adopt Eq. (2). In this approach, the elliptic equation for β^i has to be solved because we need β^i in solving hydrostatic equations (see Sec. II B).

All the basic equations are elliptic type, and hence, we have to impose appropriate boundary conditions at spatial infinity. Because of the asymptotic flatness, the boundary conditions at spatial infinity $r \to \infty$ are written as

$$\phi, \beta^i, \eta, W^i \to 0, \tag{20}$$

where we assume that the equations are solved in the inertial frame. We note that outer boundaries are located at spatial infinity in our numerical computation (cf. Sec. III). Thus, the above condition is exactly imposed.

In contrast to the case that the excision approach is adopted, we do not have to impose the inner boundary conditions in the moving-puncture approach. This could be a drawback in this approach, because we cannot impose physical boundary conditions (e.g., Killing horizon boundary condition) for the BH. However, this could be also a merit, because we have a flexibility for adjusting a quasiequilibrium state to a desired state by using this degree of freedom. In Sec. II D, we discuss this point in more detail.

B. Hydrostatic equations

Assuming that the NS is composed of an ideal fluid, we write the stress-energy tensor as

$$T_{\mu\nu} = (\rho + \rho\varepsilon + p)u_\mu u_\nu + p g_{\mu\nu}, \tag{21}$$

where ρ is the baryon rest-mass density, ε the specific internal energy, p the pressure, and u_μ the fluid four-velocity. We employ a polytropic equation of state

$$p = \kappa\rho^\Gamma, \tag{22}$$

where κ is the polytropic constant and Γ the adiabatic index. In this paper, we set $\Gamma = 2$ following previous

works [51–55]. Using the first law of thermodynamics, ε is obtained as $p/[(\Gamma-1)\rho]$, and the specific enthalpy, $h = 1+\varepsilon+p/\rho$, is given by

$$h = 1 + \kappa\frac{\Gamma}{\Gamma-1}\rho^{\Gamma-1}. \tag{23}$$

Thus, all the thermodynamic quantities are written in terms of ρ.

In the polytropic equation of state, all the dimensional quantities enter the problem only through the polytropic constant, and thus, are rescaled into a dimensionless form by normalizing in terms of the polytropic length scale,

$$R_{\rm poly} \equiv \kappa^{1/(2\Gamma-2)}. \tag{24}$$

In this paper, we present all the quantities in the dimensionless form following Refs. [51–55].

BH-NS binaries are never in a true equilibrium due to the emission of gravitational waves. However, when the orbital separation d is large enough, emission time scale of gravitational waves $t_{\rm GW}$ is much longer than the orbital period $t_{\rm orb}$ as

$$\frac{t_{\rm GW}}{t_{\rm orb}} \approx 1.1\left(\frac{d}{6m_0}\right)^{5/2}\left(\frac{m_0}{4\mu}\right), \tag{25}$$

where m_0 and μ denote the total mass and reduced mass of the binary. Thus, except for the final inspiral phase, say $d < 10m_0$, the effect of gravitational radiation reaction may be safely neglected, and the binary can be regarded to be approximately in an equilibrium state. Because the binaries in a close orbit should have a circular orbit [72,73], the fluid configuration should be in hydrostatic equilibrium in the corotating frame of the binary system. In addition, it is believed that the matter in most of the NS has the approximately irrotational velocity field for the realistic binary configurations because the viscous time scale for the angular momentum transport inside the NS is much longer than the gravitational radiation reaction time scale [74,75]. (We note that the actual NSs are known to have nonzero spin angular momenta and not exactly in the irrotational states. However, we can still approximate astrophysical NSs well with the irrotational velocity fields because their typical rotational period is 100 ms–1 s and are much longer than their typical orbital period just before mergers, $\sim 2-3$ ms, and also much longer than the dynamical time scale of the NSs, $\lesssim 1$ ms.)

The equations of relativistic hydrostatic equilibrium with the irrotational velocity field is derived independently in Refs. [76–78], which are summarized in Ref. [79]. In this formulation, one assumes the presence of a helical Killing vector

$$\xi^\mu = (\partial_t)^\mu + \Omega(\partial_\phi)^\mu. \tag{26}$$

For the irrotational velocity field, the relativistic vorticity is zero as

$$\omega_{\mu\nu} = \nabla_\mu(hu_\nu) - \nabla_\nu(hu_\mu) = 0. \tag{27}$$

Using Eq. (27) and the helical symmetric relation for the specific momentum $\mathcal{L}_\xi(hu^\mu) = 0$, we obtain the first integral of the relativistic Euler equation as

$$h\xi_\mu u^\mu = -C(=\text{const}). \tag{28}$$

To rewrite this equation into a more specific form, we decompose the four-velocity in the form

$$u^\mu = u^t(\xi^\mu + V^\mu), \tag{29}$$

where V^μ is a three-velocity (i.e., $n_\mu V^\mu = 0$) and denotes the velocity field in the comoving frame of the binary system. Then, ξ^μ is written as $\xi^\mu = u^\mu/u^t - V^\mu$. Substituting this equation into Eq. (28), we obtain [76]

$$\frac{h}{u^t} + \tilde{u}_i V^i = C, \tag{30}$$

where $\tilde{u}_i = h\gamma^\mu_i u_\mu$ denotes the three specific momentum.

The condition of irrotation, Eq. (27), implies that $\tilde{u}_i$ is written by the gradient of a velocity potential field Ψ such that

$$\tilde{u}_i = D_i\Psi, \tag{31}$$

where D_i is the covariant derivative with respect to γ_{ij}. Then, V^i is written by the velocity potential as

$$V^i = -\xi^i - \beta^i + \frac{1}{hu^t}D^i\Psi, \tag{32}$$

and also

$$u^t = \frac{1}{\alpha}[1 + h^{-2}D^k\Psi D_k\Psi]^{1/2}. \tag{33}$$

Thus, the first integral of the Euler equation is written by h, Ψ, and geometrical quantities.

The equation for the velocity potential is derived from the continuity equation, which can be written in the presence of the helical Killing vector as [76]

$$D_i(\rho\alpha u^t V^i) = 0. \tag{34}$$

Substituting Eq. (32) into Eq. (34), an elliptic-type equation for Ψ is derived to give

$$D_i[\rho\alpha\{h^{-1}D^i\Psi - u^t(\xi^i + \beta^i)\}] = 0. \tag{35}$$

This equation is also written by h, Ψ, and geometrical quantities. Thus, from the first integral of the Euler equation and Eq. (35), h and Ψ are computed, and subsequently, ρ, ε, and p are determined from the equation of state.

C. Global quantities

A quasiequilibrium state is characterized by the mass and spin of the BH, the mass and radius of the NS, and the orbital angular velocity Ω. A quasiequilibrium sequence should be a sequence as a function of Ω with constant values of the BH mass, the BH spin, and the baryon rest

mass of the NS, and with a fixed equation of state for the NS. In this paper, we assume that the BH spin is zero, and the BH mass is defined by the irreducible mass as

$$M_{\rm irr}^{\rm BH} = \sqrt{\frac{A_{\rm EH}}{16\pi}}, \tag{36}$$

where $A_{\rm EH}$ is the proper area of the event horizon. In practice, we approximate this area with that of the apparent horizon, which is computed from an integral on the apparent-horizon surface

$$A_{\rm AH} = \int_{\rm AH} \psi^4 dS, \tag{37}$$

where we use that the three-metric is conformally flat. In the moving-puncture approach, in contrast to the excision approach in which the two-sphere of the apparent horizon is readily known to be the excision surface, the apparent horizon has to be determined by a numerical computation. For finding the apparent horizon, we use the algorithm developed by Lin and Novak (see Ref. [80] for details).

The baryon rest mass of the NS is defined by

$$M_{\rm B}^{\rm NS} = \int \rho u^t \sqrt{-g} dV, \tag{38}$$

where g is the determinant of the spacetime metric $g_{\mu\nu}$. In this paper, we always present the mass in polytropic units as

$$\bar{M}_{\rm B}^{\rm NS} \equiv \frac{M_{\rm B}^{\rm NS}}{M_{\rm poly}}, \tag{39}$$

whereby $\bar{M}_{\rm B}^{\rm NS}$ is the baryon rest mass for the polytropic constant $\kappa = 1$.

In the following, we often compare numerical results with those derived by the third post-Newtonian (3PN) approximation for two points masses [81,82]. In such a case, we have to define the total mass m_0 and the reduced mass μ of the system (i.e., we have to define each mass of the binary component). For the BH mass, we use the irreducible mass. For the NS mass, we use the ADM mass of an isolated NS $M_{\rm ADM}^{\rm NS}$, with the same baryon rest mass. Thus,

$$m_0 = M_{\rm irr}^{\rm BH} + M_{\rm ADM}^{\rm NS}, \tag{40}$$

$$\mu = \frac{M_{\rm irr}^{\rm BH} M_{\rm ADM}^{\rm NS}}{m_0}. \tag{41}$$

Note that for a nonspinning BH, $M_{\rm irr}^{\rm BH}$ is equal to the ADM mass of the BH in isolation.

The ADM mass of the whole system M_0 is defined by

$$M_0 = -\frac{1}{2\pi} \oint_{r\to\infty} \partial_i \psi dS^i, \tag{42}$$

and the Komar mass is

$$M_{\rm Komar} = \frac{1}{4\pi} \oint_{r\to\infty} \partial_i \alpha dS^i, \tag{43}$$

$$= \frac{1}{4\pi} \oint_{r\to\infty} (\partial_i \Phi - \partial_i \psi) dS^i. \tag{44}$$

Note that equating these two masses results in Eq. (12). We also define the binding energy of the binary as

$$E_b = M_0 - m_0. \tag{45}$$

The ADM linear momentum of the system is

$$P_i = \frac{1}{8\pi} \oint_{r\to\infty} K_{ij} dS^j, \tag{46}$$

where we assume the maximal slicing $K = 0$. This is set to be zero in the present work. The angular momentum of the system around the center of mass of the binary may be defined by

$$J_i = \frac{1}{16\pi} \epsilon_{ijk} \oint_{r\to\infty} (X^j K^{kl} - X^k K^{jl}) dS_l, \tag{47}$$

where X^i is the coordinate vector from the center of mass.

D. Free parameters

To compute a quasiequilibrium configuration for a given equation of state, we have to fix free parameters. Each configuration is determined when we fix (i) the baryon rest mass of the NS, $M_{\rm B}^{\rm NS}$, (ii) the mass ratio, Q, or equivalently, the irreducible mass of the BH, $M_{\rm irr}^{\rm BH}$, and (iii) the separation between the BH and the NS, d. Then, the other parameters such as $M_{\rm P}$, M_Φ, and $P_i^{\rm BH}$ are automatically determined in the computation: The puncture mass $M_{\rm P}$ is arranged to give a desired irreducible mass, the mass parameter M_Φ is determined by the condition that the ADM mass and the Komar mass agree (see Eq. (12)), and the linear momentum of the BH, $P_i^{\rm BH}$, is determined by the condition that the total linear momentum of the system should vanish [see Eq. (15)].

There are also free parameters associated with the configuration of the NS; the integration constant C, which appears in the first integral of the Euler Eq. (30), and the angular velocity of the binary Ω. These are determined by fixing the configuration of the binary and the baryon rest mass of the NS. Specifically, we fix the rest mass of the NS to determine C and fix the location of the center of the NS to determine Ω. Here, the center of the NS is defined as the position at which the following condition is satisfied [53,79]:

$$\left.\frac{\partial \ln h}{\partial X}\right|_{(X_{\rm NS}, Y_{\rm NS}, 0)} = 0, \tag{48}$$

where $X_{\rm NS}$ and $Y_{\rm NS}$ are the distances in the x and y directions from the center of the NS to the rotational axis, respectively. In the actual calculation, we arrange the value of the specific enthalpy at the center of the NS,

h_c, instead of C, since it is easier to implement. The value of C is determined by h_c and the values of metric quantities at the center of the NS.

The final remaining task in the moving-puncture framework is to determine the center of mass of the system. The issue in this framework is that we do not have any natural, physical condition for determining it. (By contrast, the condition is automatically derived in the excision framework [51–55], although it is not clear whether the resulting quasiequilibrium is a quasicircular state [66].) In our previous paper [56,57], we employed a condition that the dipole part of ψ at spatial infinity is zero (hereafter we refer to this condition as ''dipole condition''). However, we found that in this condition, the angular momentum derived for a close orbit of $\Omega m_0 \gtrsim 0.03$ is by $\sim 2\%$ smaller than that derived by the 3PN approximation [81,82] for $Q = 3$. Because the 3PN approximation should be an excellent approximation of general relativity for a fairly distant orbit as $\Omega m_0 \approx 0.03$, the obtained initial data deviates from the true quasicircular state, and hence, the initial orbit would be eccentric.

In the subsequent work [58], we adopted a condition that the azimuthal component of the shift vector β^φ at the location of the puncture ($\boldsymbol{r} = \boldsymbol{r}_{\rm P}$) is equal to $-\Omega$; i.e., we imposed a corotating gauge condition at the location of the puncture. In the following, we refer to this condition as the ''β^φ condition.'' In this paper, we first present the numerical results in the latter condition because it is a physical condition and gives a slightly better result than the dipole condition does.

As shown in Sec. IV, however, the angular momentum derived for a close orbit of $\Omega m_0 \gtrsim 0.03$ in this method is still by $\sim 2\%$ smaller than that derived by the 3PN relation for a large mass ratio $Q \geq 2$. The disagreement is larger for the larger mass ratio. Such initial conditions are likely to deviate from the true quasicircular state and hence the orbital eccentricity is large (e.g. Sec. IV C of Ref. [61] for numerical evolution of such initial data). This also suggests that the β^φ condition is not suitable for deriving realistic quasicircular states.

In this paper, we further propose a new condition in which the center of mass is determined in a phenomenological manner: We impose the condition that the total angular momentum of the system for a given value of Ωm_0 agrees with that derived by the 3PN approximation. This can be achieved by appropriately choosing the position of the center of mass. With this method, the drawback in the previous two methods (i.e., the angular momentum becomes smaller than the expected value) is overcome. We refer to this method as ''3PN-J condition'' in the following.

III. NUMERICAL METHODS

In this section, we summarize our numerical scheme for computing a quasiequilibrium state.

A. Methods of computation

Our numerical code is based on the spectral methods library LORENE [83]. In the spectral methods, any quantity is denoted by the expansion into a complete set of polynomials. The feature in the spectral methods is that the error of this expansion decreases exponentially as the number of the used complete set of polynomials increases, at least for continuous functions. Furthermore, irregular functions like the rest-mass density of the NS, for which the spatial derivative jumps at its surface and is not straightforward to expand into a complete set of polynomials (known as ''Gibbs phenomenon''), can be treated appropriately by employing a multidomain spectral method. We use two sets of spherical-like computational domains, each of which is centered on each object. The one for which the domain center is located at the puncture is composed of one nucleus, which is sphere at the center, several shells, and the external domain, which extends to spatial infinity. The other has almost the same structure, except that the outer boundary of the nucleus is deformed to fit the surface of the NS. With this computational domain, irregular profiles of the density are contained only in the domain boundary, and hence, no Gibbs phenomenon arises, if the density decreases sufficiently smooth at the boundary, e.g., for the $\Gamma = 2$ polytropic equation of state. We also locate the outer boundaries at spatial infinity by employing a radial coordinate, which is obtained by a transformation $u = 1/r$ in the outermost domain. With this treatment, the exact boundary conditions at spatial infinity can be imposed. Because the multidomain method is employed and field equations are solved for many domains, we split the field equations into the ''BH part'' and the ''NS part'' like the way described in Appendix. A of Ref. [53].

Our computational domains centered on the BH are divided into 8 domains and each of them is covered by $N_r \times N_\theta \times N_\phi = 41 \times 33 \times 32$ collocation points. Similarly, the domains for the NS are divided into 6 domains and each of them is covered by $N_r \times N_\theta \times N_\phi = 25 \times 17 \times 16$ collocation points. Here, N_r, N_θ, and N_ϕ are the number of collocation points for radial, polar, and azimuthal directions, respectively.

B. Iteration procedure

Numerical solutions of quasiequilibrium states are obtained by iteratively solving the basic equations described in Sec. II. Here, we briefly summarize our procedure of the iteration. As described in Sec. II D, the calculation should be performed to give correct $M_{\rm B}^{\rm NS}$, $M_{\rm irr}^{\rm BH}$, and d.

First of all, we need to prepare an initial trial solution for the iterative procedure. For this purpose, we superimpose a Schwarzschild solution in the isotropic coordinates and a spherical NS. Then, our iterative procedure is as follows:

(1) Determine the orbital angular velocity Ω by using Eq. (48).

(2) Determine the location of the center of mass (rotational axis) of the system. Because the coordinate separation between two objects are initially given, the positions of both objects relative to the center of mass are also determined.
(3) Solve the equations described in Secs. II A and II B in each domain.
(4) Adjust $M_{\rm P}$ to fix the irreducible mass of the BH to a desirable value. After this procedure, determine M_Φ so that the condition (12) is satisfied.

Adjust the maximum enthalpy of the NS, h_c, at the center of the NS, to fix the baryon rest mass of the NS. We repeat this procedure until a sufficient convergence is achieved. As a measure of the convergence, we monitor the relative difference between the enthalpy field of successive steps. Typically, we stop the iteration when the following condition is satisfied:

$$\sum_{i,j,k} |1 - h^n_{i,j,k}/h^{n-1}_{i,j,k}| \le 10^{-6}, \tag{49}$$

where n denotes the iteration step, and (i, j, k) the collocation points of (r, θ, φ).

IV. NUMERICAL RESULTS

Throughout this paper, we characterize a quasiequilibrium sequence by two parameters; the baryon rest mass of the NS, $\bar{M}^{\rm NS}_{\rm B}$, and the ratio of the irreducible mass of the BH to the ADM mass of the NS in isolation, $Q \equiv M^{\rm BH}_{\rm irr}/M^{\rm NS}_{\rm ADM,0}$. We focus on the sequences of $\bar{M}^{\rm NS}_{\rm B} = 0.14$, 0.15, and 0.16 following Ref. [54]. For these cases, the compactness of the NSs is $\mathcal{C} = 0.1321$, 0.1452, and 0.1600, respectively, implying that we choose moderately large values for the compactness. Note that the maximum value of $\bar{M}^{\rm NS}_{\rm B}$ is about 0.18 for the $\Gamma = 2$ polytropic equation of state. At that value of $\bar{M}^{\rm NS}_{\rm B}$, the compactness is about $\mathcal{C} = 0.21$. Here, the compactness is defined by

$$\mathcal{C} \equiv \frac{M^{\rm NS}_{\rm ADM,0}}{R_0}, \tag{50}$$

where R_0 is the circumferential radius of the NS in isolation. For the mass ratio, we choose $1 \le Q \le 5$.

A. Binding energy and total angular momentum in the β^φ condition

Figure 1 plots the binding energy and total angular momentum as functions of Ωm_0 for $Q = 1$, 3, 5, and $\bar{M}^{\rm NS}_{\rm B} = 0.15$ in the β^φ condition. For comparison, the results in the excision approach [54] and in the 3PN approximation are also plotted.

For large orbital separations (small values of $\Omega m_0 \lesssim 0.02$), the results obtained in the moving-puncture method (with the β^φ condition) agree well with those derived by the 3PN approximation and in the excision approach [54] irrespective of the mass ratio. For smaller separations, however, the degree of agreement among three results depends on the mass ratio. For $Q = 1$, three results agree within $\sim$1% error. By contrast, for $Q = 3$ and 5, a significant deviation of order $\sim$10% arises among three results for $\Omega m_0 \gtrsim 0.03$. In particular, for $Q = 5$, the results in the moving-puncture approach (with the β^φ condition) disagree significantly with other two results (see lower panels of Fig. 1). Because the tidal effect does not play an important role and the orbital velocity is at most $\sim 0.1c$ for a fairly distant orbit of $\Omega m_0 \sim 0.03$, the numerical results should agree with the results in the 3PN approximation, at least approximately. This implies that the quasiequilibrium state obtained in the moving-puncture approach (with the β^φ condition) is not in a quasicircular orbit for the close orbit of $\Omega m_0 \gtrsim 0.03$ and for $Q \ge 3$; it would be an eccentric orbit. Also, quasiequilibrium states in this moving-puncture approach appear to be inferior to those in the excision approach in that they show systematic deviations from other two results.

One possible reason for this deviation may stem from the condition for determining the center of mass of the system. This point is explored in detail in Sec. IV B. Another possible reason is that the BH might have nonzero spin in the present approach. Indeed, in the excision framework, it has been found that the "leading-order approximation" leads to a slightly spinning BH [84,85]. To obtain a strictly nonspinning BH, a computation has to be performed with an improved method for determining the spin angular velocity of the BH. Motivated by this fact, we measured the spin of the BH using a method proposed by Cook and Whiting [86]. However, we find that the BH has negligible spin of order $S/M^2_{\rm irr} \lesssim 10^{-5}$, and therefore, the deviation between the results in the moving-puncture method (with the β^φ condition) and others is not caused by the spin of the BH.

Numerical results of binding energy and total angular momentum in the moving-puncture method as a function of Ωm_0 for different compactness of the NS are plotted in Fig. 2. This shows that the feature of the results described above holds irrespective of the compactness of the NS. For smaller values of the compactness (i.e., for smaller values of $\bar{M}^{\rm NS}_{\rm B}$), the binding energy and the angular momentum are slightly larger for a given value of $\Omega m_0 \gtrsim 0.04$. This is due to the fact that for less compact NSs, the tidal-deformation effect on the NS plays an important role in increasing these quantities in close orbits [87]. We note that, in the moving-puncture approach, it is possible to obtain the sequences of quasiequilibria for the NSs with the compactness $\mathcal{C} \lesssim 0.18$ for the $\Gamma = 2$ polytropic equation of state. Meanwhile, our computations do not show adequate convergence for the binaries containing more compact NSs, because such NSs are close to the most compact ones allowed by the given equation of state, $\mathcal{C} \sim 0.21$ in this case, and are difficult to compute accurately. For the $\Gamma > 2$ equation of state for which the maximum

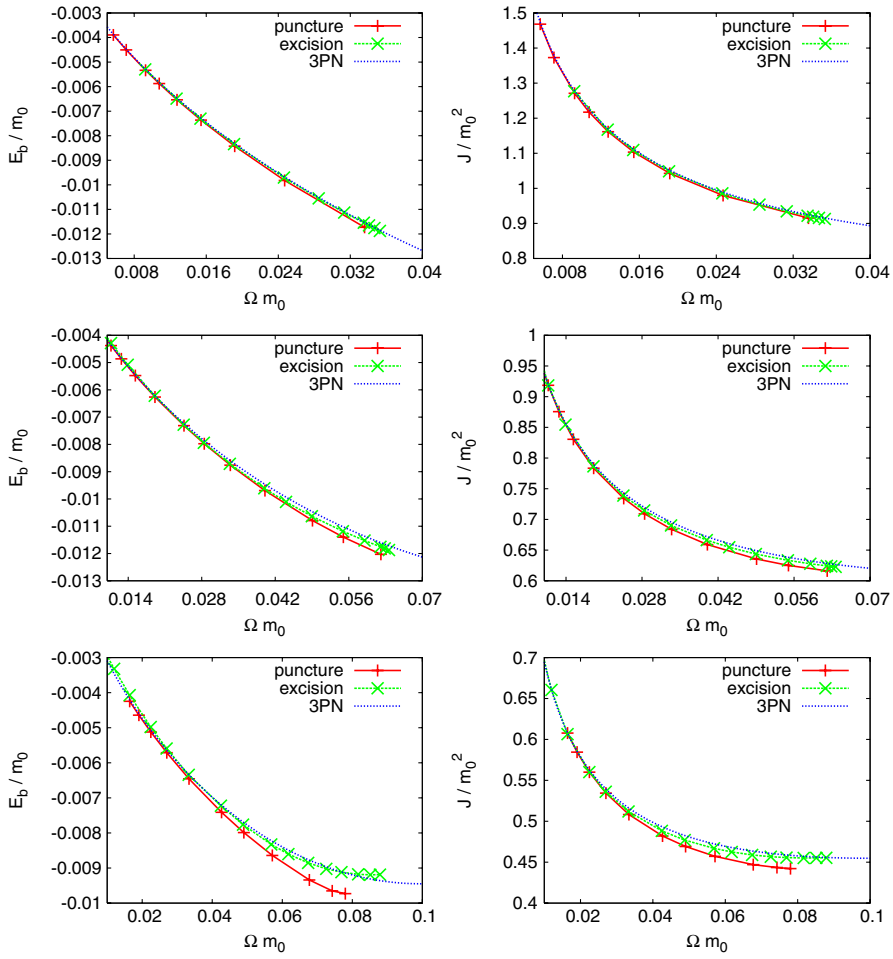

FIG. 1 (color online). Left panels: Binding energy E_b/m_0 as a function of Ωm_0 for $\bar{M}_{\rm B}^{\rm NS} = 0.15$ and $Q = 1$ (upper panel), 3 (middle panel), and 5 (lower panel). The solid (red) and dashed (green) curves show the results obtained in the moving-puncture method with the β^φ condition and in the excision method [54], respectively. The dotted (blue) curve denotes the result in the 3PN approximation [81]. Right panels: The same as the left panels but for the total angular momentum J/m_0^2 as a function of Ωm_0.

compactness is larger than 0.21, we are able to obtain NSs of compactness $\sim$0.2.

Before closing this subsection, we point out the following issue found from Fig. 1: The angular momentum for a given value of Ωm_0 in the numerical results is always smaller than that in the 3PN approximation for $\Omega m_0 \gtrsim 0.03$. This holds for the results not only in the moving-puncture approach (with the β^φ condition) but also in the excision approach. For a fairly distant orbit of $\Omega m_0 \sim 0.03$, the 3PN approximation should be an excellent approximation of general relativity, and hence, provides a highly accurate result. This implies that angular momen-

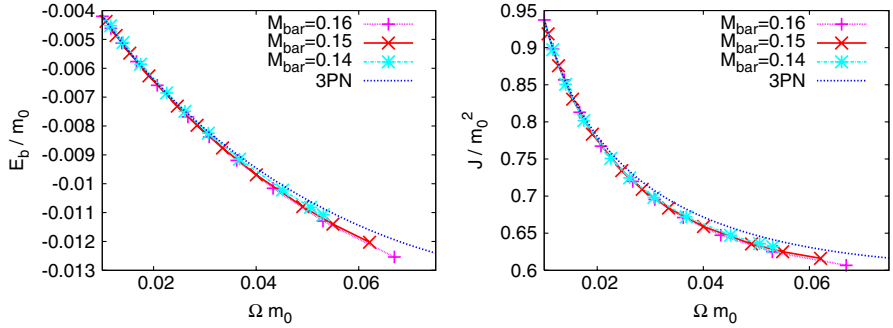

FIG. 2 (color online). The same as Fig. 1 but for $\bar{M}_{\rm B}^{\rm NS} = 0.14$, 0.15, and 0.16, and for $Q = 3$ in the moving-puncture method.

tum in the numerical results is smaller than that for the real quasicircular state. As shown in Sec. IV C, this is indeed the case. Figure 1 indicates that for numerical simulation, these quasiequilibria may not be good initial conditions, and an improved quasiequilibrium would be favorable as the initial condition of numerical simulation.

B. Effect of the center of mass

As mentioned in Sec. II D, we have no definitive guidance for determining the position of the center of mass in the moving-puncture framework. In the excision framework, the position is automatically determined so that the ADM linear momenta should vanish. By contrast, in the moving-puncture framework, this condition was already used to determine another free parameter, $P_i^{\rm BH}$.

As described in Sec. II D, we have at least three methods for determining the center of mass, and numerical results depend strongly on them. In this subsection, we compare these numerical results.

In Fig. 3, we show sequences of $\bar{M}_{\rm B}^{\rm NS} = 0.15$ for $Q = 1$, 3, and 5 obtained by three different methods for the center of mass. "shift," "dipole," and "set to 3PN" denote the results derived in the β^{φ}, dipole, and 3PN-J conditions, respectively.

The numerical results in the β^{φ} and dipole conditions show a similar behavior. For $Q = 1$, these results agree approximately with those in the 3PN approximation, and for $Q = 3$ and 5, the deviation from the 3PN results becomes significant as pointed out in Sec. IV A. The deviation from the 3PN results is slightly smaller for the results in the β^{φ} condition for $Q = 3$ and 5 than those in the dipole condition. This indicates that the β^{φ} condition is slightly better for computing unequal-mass BH-NS binaries in quasiequilibrium, although the deviation from the 3PN results is larger than 1% for $\Omega m_0 \gtrsim 0.03$.

The sequence obtained in the 3PN-J condition shows rather different behavior. By definition, the angular momentum agrees with the results obtained in the 3PN approximation. As a result, however, the binding energy

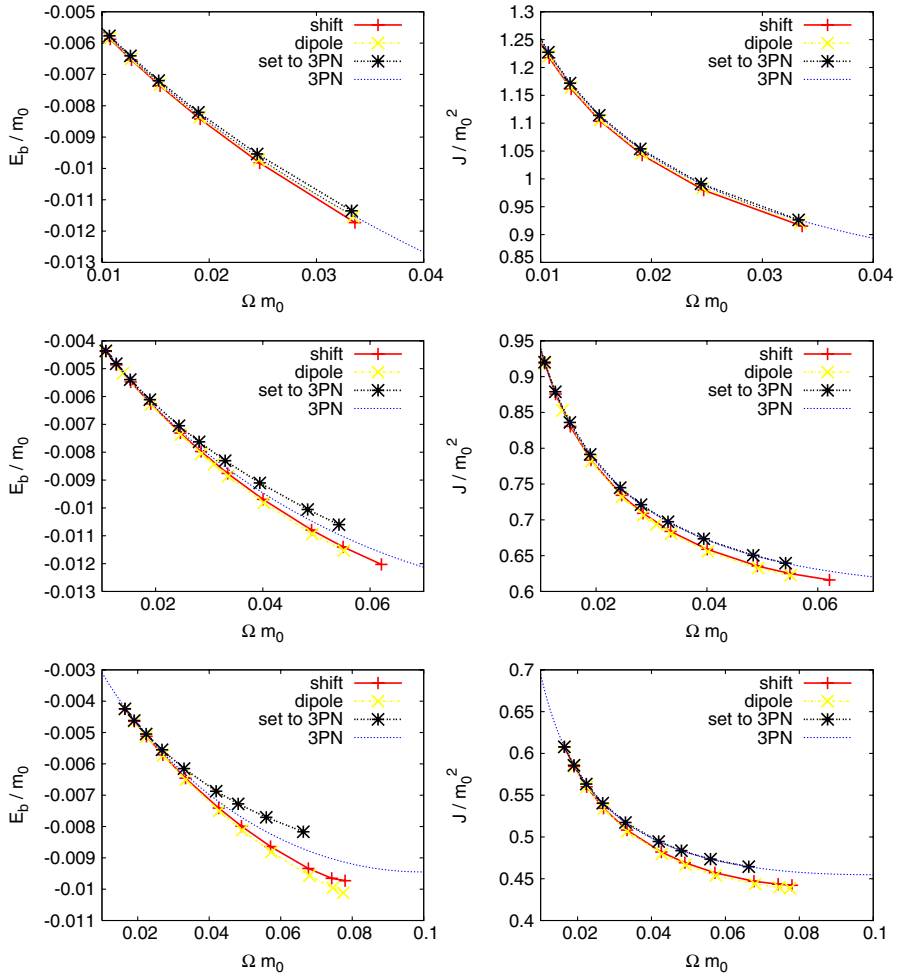

FIG. 3 (color online). Left panels: Binding energy E/m_0 as a function of Ωm_0 for $\bar{M}_{\rm B}^{\rm NS} = 0.15$ and $Q = 1$, 3, and 5 in the moving-puncture approach with three different conditions for determining the center of mass of system. The dotted curve denotes the result in the 3PN approximation. Right panels: The same as the left panels but for the total angular momentum J/m_0^2 as a function of Ωm_0.

becomes larger than that in the 3PN approximation, in contrast to the results in other two methods. A possible interpretation for the excess of the binding energy is that junk gravitational radiation or nonstationary kinetic energy (e.g., oscillation of a nonstationary BH) are included in the data. However, if these nonstationary components are radiated away during numerical evolution, this initial data could provide an approximate quasicircular state.

C. Assessing quality of quasiequilibrium by numerical simulation

The results presented in the previous subsection show that the quasiequilibrium states computed in three conditions of the moving-puncture approach are not in quasicircular orbits for $Q \neq 1$, but rather are likely to be in eccentric orbits. However, if the eccentricity is small enough, it quickly approaches zero during evolution, resulting in that a realistic binary, i.e., a (n approximately) quasicircular state, is provided. To assess circularity of quasiequilibrium states as the initial condition of numerical relativity, we performed a numerical simulation, choosing a binary of $\bar{M}_{\rm B}^{\rm NS} = 0.15$ and $Q = 3$ and 5. In this subsection, we present the results of the numerical simulation. In this experiment, we adopt the initial data obtained in the β^{φ} and 3PN-J conditions of the moving-puncture approach. For all the data, the angular velocity is chosen to be $\Omega m_0 \approx 0.033$. The numerical simulation was performed using our code SACRA, in which an adaptive mesh refinement algorithm is implemented. The formulation, gauge condition, and numerical scheme adopted in SACRA are the same as described in Ref. [61].

Figure 4 plots evolution of the orbital angular velocity as a function of retarded time. Here, the angular velocity is calculated by the quadrupole mode of gravitational waveforms by [44]

$$\Omega(t) = \frac{1}{2}\frac{|\Psi_4(l=m=2)|}{|\int dt \Psi_4(l=m=2)|}, \tag{51}$$

where Ψ_4 denotes the outgoing part of the Newman-Penrose quantity. This figure illustrates that the orbit of the binaries is eccentric for all the cases, reflecting the fact that the circular orbit is not provided initially. For the initial data obtained in the β^{φ} condition, the eccentricity appears to be of order 0.1. Moreover, the eccentricity does not reduce to zero even at the onset of merger. We note that for these cases, the binary spends in the inspiral phase for 4–5 orbits before the onset of the merger. Nevertheless, the eccentricity is not sufficiently reduced by the gravitation radiation reaction and a quasicircular orbit is not achieved before the merger. The reason for this is that the initial eccentricity is too large.

By contrast, for the initial data obtained in the 3PN-J condition, the eccentricity appears to be much smaller than those for other two cases. This suggests that the initial eccentricity is smaller.

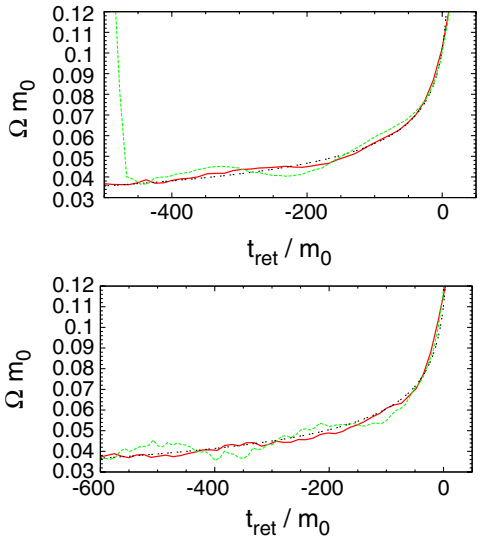

FIG. 4 (color online). Angular velocity of gravitational waveforms as a function of retarded time $t_{\rm ret}$ for $Q = 3$ (left) and $Q = 5$ (right) and for $\mathcal{C} = 0.15$. $t_{\rm ret} = 0$ approximately denotes the merger time. The solid and dashed curves denote the results in the 3PN-J condition and the β^{φ} condition, respectively. The dot-dotted curve is the result in the 3PN approximation (Taylor T4 formula; e.g., Ref. [49]).

By comparing the numerical results with that obtained in the 3PN approximation (dot-dotted curve), we find that the modulation amplitude of the angular velocity is $\Delta(\Omega m_0) \approx 0.004$–$0.006$ even just before the merger (at $\Omega m_0 \sim 0.05$) in the β^{φ} condition. Eccentricity of the orbit is approximately estimated to be $2\Delta\Omega/3\Omega$ for a slightly eccentric orbit. Thus, the eccentricity for these cases is $\sim$0.05–0.08.

By contrast, the modulation amplitude is at most $\Delta(\Omega m_0) \approx 0.003$ for the initial data given in the 3PN-J condition. Furthermore, the modulation is suppressed to be $\lesssim 0.001$ just before the onset of merger ($\Omega m_0 \gtrsim 0.05$) in this case, indicating that the eccentricity is $\lesssim 0.01$. This shows that the moving-puncture approach with the 3PN-J condition is superior for providing the initial data for the numerical-relativity simulation.

D. Mass-shedding limit

As analyzed in detail in Refs. [53,54], the NS is strongly subject to tidal deformation by a companion BH outside their innermost stable circular orbit (ISCO), if the mass ratio of the system is small enough or the radius of the NS is large enough. In the case that the tidal field of the BH is strong enough, the Lagrangian point enters inside the surface of the NS. Then the NS cannot be in equilibrium any longer because mass shedding occurs from the inner edge of the NS's surface. We here determine the condition for the onset of mass shedding in the moving-puncture approach with the β^{φ} condition. As shown in the previous two subsections, the quasiequilibrium states obtained in

this approach are not quasicircular states but slightly eccentric ones. This seems to be also the case for the quasiequilibrium states obtained in the excision approach employed in Refs. [53,54]. Even though there exists nonzero eccentricity in the data, we think that it still deserves to reinvestigate the mass-shedding limit in the moving-puncture approach and to compare the results with those obtained in the excision approach.

In the spectral methods one cannot determine any equilibrium configuration for a star with irregular surface shape (i.e., with a cusp). At the onset of mass shedding, the inner edge of the NS has a cusp, and hence, it is not possible to accurately compute quasiequilibrium states of the NS in close orbits with a BH. Thus, we infer the orbital separation (or angular velocity) at the onset of mass shedding from quasiequilibrium states of slightly more distant orbits than the mass-shedding configuration has. For this procedure, we define a mass-shedding indicator χ [79] as the fraction of the radial derivative of the enthalpy at the NS surface,

$$\chi \equiv \left(\frac{(\partial(\ln h)/\partial r)_{\rm eq}}{(\partial(\ln h)/\partial r)_{\rm pole}} \right), \tag{52}$$

where subscripts "eq" and "pole" imply that the partial derivative is taken with respect to the radial direction connecting the centers of the NS and BH in the equatorial plane and along the polar direction, respectively. For the infinite separation, the NS becomes spherical and $\chi = 1$, whereas χ decreases with increasing the degree of tidal deformation and eventually becomes zero at the onset of mass shedding. Because our code does not converge to give quasiequilibrium for $\chi \to 0$, we first compute a sequence of χ for close orbits, and then, derive a fitting formula for the curve of χ as a function of orbital separation. By using this fitting formula, we determine the orbital separation for $\chi = 0$.

Figure 5 plots the mass-shedding indicator χ as a function of Ωm_0 for the sequences of $\bar{M}_{\rm B}^{\rm NS} = 0.15$, and $Q = 3$ and 5. For comparison, we also plot the results obtained in the excision method. This figure shows that the curves obtained in the moving-puncture approach agree approximately with those in the excision approach. This indicates that the mass-shedding limit would be determined with a small error even in the presence of spurious eccentricity of order ~ 0.1.

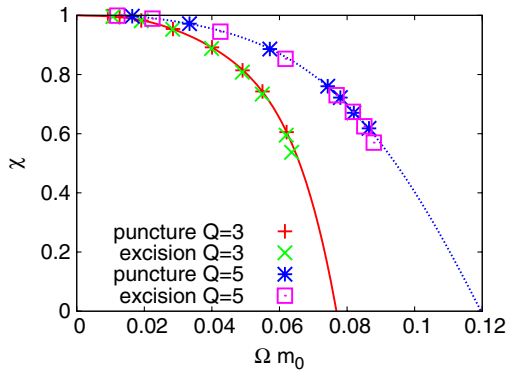

FIG. 5 (color online). The mass-shedding parameter χ versus Ωm_0 for the sequences of $\bar{M}_{\rm B}^{\rm NS} = 0.15$, and $Q = 3$ and 5. We also show the results obtained in the excision method [54].

In the works performed in the excision approach [53,54], the ISCO is also determined by finding the extremum of the binding energy (or the total angular momentum). They find that for $\bar{M}_{\rm B}^{\rm NS} = 0.15$ and $Q = 5$, the binary reaches the ISCO before the mass-shedding limit is reached, whereas for $Q = 3$, the mass shedding occurs before the binary reaches the ISCO. In the present moving-puncture approach, we do not find any extremum even for $Q = 5$. This is primarily due to the fact that this approach is not suitable for computing quasicircular states for very close orbits.

We also compare our results of mass-shedding limit with that of the dynamical simulations [63]. Since it is difficult to determine the onset of mass shedding in the dynamical simulations, we determine the value of Ωm_0 at the time when the matter in the NSs is first swallowed by the BHs. For the case of $Q = 3$, the matter is swallowed by the BH at $\Omega m_0 \sim 0.09$, which is larger than the mass-shedding limit obtained in this paper and in other works [53,54]. However, two results are consistent because the mass shedding occurs before the matter falls into the BH; $\Omega m_0 \sim 0.09$ shows the upper limit for the value of Ωm_0 at the mass shedding. On the other hand, for the case of $Q = 5$, the matter is first swallowed by the BH at $\Omega m_0 \sim 0.1$. This simply implies that the binary reaches the ISCO at $\Omega m_0 \sim 0.1$.

V. SUMMARY

We numerically derive new general relativistic quasiequilibrium states of BH-NS binaries in the moving-puncture approach. Basic equations for gravitational fields are solved in the mixture of conformal thin-sandwich decomposition and conformal transverse-traceless decomposition, and hydrostatic equations are solved under the assumption of irrotational velocity field and employing the polytropic equation of state.

In the moving-puncture approach, no definitive physical condition is present for determining the center of mass of the system. We propose three conditions for defining the center of mass and compare the resulting quasiequilibrium states with the 3PN results and results obtained in the excision approach.

Sequences of quasiequilibrium states are computed for the mass ratio $1 \le Q \le 5$, and for $\bar{M}_{\rm B}^{\rm NS} = 0.14$, 0.15, and 0.16 (each of which corresponds to the compactness $\mathcal{C} = 0.1321$, 0.1452, and 0.1600). For large orbital separation with $\Omega m_0 \lesssim 0.02$, the results in the moving-puncture approach agree with the results obtained in the 3PN approximation and in the excision approach, irrespective of the

conditions for determining the center of mass and irrespective of the mass ratio of the binary. Thus, such quasiequilibrium states are likely to be (at least approximately) quasicircular orbits for which the eccentricity is approximately zero. By contrast, for small orbital separation with $\Omega m_0 \gtrsim 0.03$, the results in the moving-puncture approach with β^φ and dipole conditions for determining the center of mass systematically deviate from the 3PN results, in particular, for large mass ratio. The angular momentum for the resulting quasiequilibrium is always smaller than that in the 3PN results, and hence, the quasiequilibrium appears to contain a nonzero eccentricity. As an alternative method for determining the center of mass, we propose a method in which it is determined by requiring that the angular momentum for a give value of the angular velocity should agree with that in the 3PN approximation.

To assess the circularity of the quasiequilibria computed in different approaches, we performed numerical simulation for a chosen model; $\bar{M}_{\rm B}^{\rm NS} = 0.15$, $Q = 3$ and 5, and $\Omega m_0 \approx 0.033$. The numerical simulation was performed for two quasiequilibrium states prepared in the β^φ and 3PN-J conditions. We find that the quasiequilibria computed in the β^φ condition have eccentricity of $\sim$0.05–0.08. During the simulation, the eccentricity reduces due to gravitational radiation reaction, but in $\sim$4–5 orbits, it does not reduce to $\lesssim 0.01$ even at the onset of merger. By contrast, the eccentricity of the quasiequilibrium state computed in the 3PN-J condition is by a factor of $\sim$2 smaller. For such case, the eccentricity reduces approximately to $\sim$0.01 in $\sim$4–5 orbits, and the resulting eccentricity at the onset of merger appears to be $\lesssim 0.01$. Therefore, with the quasiequilibrium prepared in the 3PN-J condition, it is feasible to compute a realistic gravitational waveform at least from the final a few inspiral orbits to the merger phase (see an accompany paper [63] for detailed numerical results).

In this paper, we study BH-NS binaries in which the BH is not spinning. If the BH has a substantial spin, the quasiequilibrium state of BH-NS binaries will be modified by the spin-orbit interaction effect (e.g., Ref. [82]). We plan to study the effect of the BH spin in the next work.

ACKNOWLEDGMENTS

Numerical computation of quasiequilibrium states is performed using the free library LORENE [83]. We thank members in the Meudon Relativity Group for developing LORENE. This work was supported by the Grant-in-Aid for Scientific Research (No. 19540263), by the Grant-in-Aid for Scientific Research on Innovative Areas (No. 20105004) of the Japanese Ministry of Education, Culture, Sports, Science and Technology and by the Grand-in-Aid for JSPS. This work was also supported in part by NSF Grant No. PHY-0503366.

[1] LIGO website, http://www.ligo.caltech.edu/.
[2] VIRGO website, http://www.virgo.infn.it/.
[3] GEO600 website, http://geo600.aei.mpg.de/.
[4] TAMA300 website, http://tamago.mtk.nao.ac.jp/.
[5] R. Voss and T. M. Tauris, Mon. Not. R. Astron. Soc. **342**, 1169 (2003).
[6] V. Kalogera, K. Belczynski, C. Kim, R. O'Shaughnessy, and B. Willems, Phys. Rep. **442**, 75 (2007).
[7] K. Belczynski, R. E. Taam, V. Kalogera, F. A. Rasio, and T. Bulik, Astrophys. J. **662**, 504 (2007).
[8] E. Nakar, Phys. Rep. **442**, 166 (2007).
[9] W. H. Lee and E. Ramirez-Ruiz, New J. Phys. **9**, 17 (2007).
[10] R. Narayan, B. Paczyński, and T. Piran, Astrophys. J. **395**, L83 (1992).
[11] C. L. Fryer, S. E. Woosley, M. Herant, and M. E. Davies, Astrophys. J. **520**, 650 (1999).
[12] M. Shibata and K. Uryū, Phys. Rev. D **61**, 064001 (2000).
[13] M. Shibata and K. Uryū, Prog. Theor. Phys. **107**, 265 (2002).
[14] M. Shibata, K. Taniguchi, and K. Uryū, Phys. Rev. D **68**, 084020 (2003).
[15] M. Shibata, K. Taniguchi, and K. Uryū, Phys. Rev. D **71**, 084021 (2005).
[16] M. Shibata and K. Taniguchi, Phys. Rev. D **73**, 064027 (2006).
[17] M. D. Duez, P. Marronetti, S. L. Shapiro, and T. W. Baumgarte, Phys. Rev. D **67**, 024004 (2003).
[18] M. Miller, P. Gressman, and W.-M. Suen, Phys. Rev. D **69**, 064026 (2004).
[19] M. Anderson, E. W. Hirschmann, L. Lehner, S. L. Liebling, P. M. Motl, D. Neilsen, C. Palenzuela, and J. E. Tohline, Phys. Rev. D **77**, 024006 (2008).
[20] Y.-T. Liu, S. L. Shapiro, Z. B. Etienne, and K. Taniguchi, Phys. Rev. D **78**, 024012 (2008).
[21] L. Baiotti, B. Giacomazzo, and L. Rezzolla, Phys. Rev. D **78**, 084033 (2008).
[22] F. Pretorius, Phys. Rev. Lett. **95**, 121101 (2005).
[23] F. Pretorius, Classical Quantum Gravity **23**, S529 (2006).
[24] M. Campanelli, C. O. Lousto, P. Marronetti, and Y. Zlochower, Phys. Rev. Lett. **96**, 111101 (2006).
[25] M. Campanelli, C. O. Lousto, Y. Zlochower, and D. Merritt, Phys. Rev. Lett. **98**, 231102 (2007).
[26] M. Campanelli, C. O. Lousto, and Y. Zlochower, Phys. Rev. D **73**, 061501(R) (2006).
[27] M. Campanelli, C. O. Lousto, and Y. Zlochower, Phys. Rev. D **74**, 084023 (2006).
[28] J. G. Baker, J. Centrella, D.-I. Choi, M. Koppitz, and J. van Meter, Phys. Rev. Lett. **96**, 111102 (2006).
[29] J. G. Baker, J. Centrella, D.-I. Choi, M. Koppitz, and J. van

Meter, Phys. Rev. D **73**, 104002 (2006).
[30] J. G. Baker, J. Centrella, D.-I. Choi, M. Koppitz, J. van Meter, and M. C. Miller, Astrophys. J. **653**, L93 (2006).
[31] P. Diener, F. Herrmann, D. Pollney, E. Schnetter, E. Seidel, R. Takahashi, J. Thornburg, and J. Ventrella, Phys. Rev. Lett. **96**, 121101 (2006).
[32] L. Rezzolla, P. Diener, E. N. Dorband, D. Pollney, C. Reisswig, E. Schnetter, and J. Seiler, Astrophys. J. **674**, L29 (2008).
[33] L. Rezzolla, E. N. Dorband, C. Reisswig, P. Diener, D. Pollney, E. Schnetter, and B. Szilágyi, Astrophys. J. **679**, 1422 (2008).
[34] D. Pollney *et al.*, Phys. Rev. D **76**, 124002 (2007).
[35] M. Koppitz, D. Pollney, C. Reisswig, L. Rezzolla, J. Thornburg, P. Diener, and E. Schnetter, Phys. Rev. Lett. **99**, 041102 (2007).
[36] M. A. Scheel, H. P. Pfeiffer, L. Lindblom, L. E. Kidder, O. Rinne, and S. A. Teukolsky, Phys. Rev. D **74**, 104006 (2006).
[37] B. Brügmann, J. A. Gonzalez, M. Hannam, S. Husa, U. Sperhake, and W. Tichy, Phys. Rev. D **77**, 024027 (2008).
[38] B. Szilágyi, D. Pollney, L. Rezzolla, J. Thornburg, and J. Winicour, Classical Quantum Gravity**24**, S275 (2007).
[39] J. G. Baker, M. Campanelli, F. Pretorius, and Y. Zlochower, Classical Quantum Gravity **24**, S25 (2007).
[40] L. Herrmann, I. Hinder, D. Shoemaker, P. Laguna, and R. A. Matzner, Astrophys. J. **661**, 430 (2007).
[41] C. F. Sopuerta, N. Yunes, and P. Laguna, Astrophys. J. **656**, L9 (2007).
[42] J. A. Gonzalez, U. Sperhake, B. Brügmann, M. Hannam, and S. Husa, Phys. Rev. Lett. **98**, 091101 (2007).
[43] J. A. Gonzalez, M. Hannam, U. Sperhake, B. Brügmann, and S. Husa, Phys. Rev. Lett. **98**, 231101 (2007).
[44] A. Buonanno, G. B. Cook, and F. Pretorius, Phys. Rev. D **75**, 124018 (2007).
[45] J. G. Baker, S. T. McWilliams, J. R. van Meter, J. Centrella, D.-I. Choi, B. J. Kelly, and M. Koppitz, Phys. Rev. D **75**, 124024 (2007).
[46] H. P. Pfeiffer, D. A. Brown, L. E. Kidder, L. Lindblom, G. Lovelace, and M. A. Scheel, Classical Quantum Gravity **24**, S59 (2007).
[47] M. Hannam, S. Husa, J. A. González, U. Sperhake, and B. Brügmann, Phys. Rev. D **77**, 044020 (2008).
[48] P. Marronetti, W. Tichy, B. Brügmann, J. A. González, and U. Sperhake, Phys. Rev. D **77**, 064010 (2008).
[49] M. Boyle, D. A. Brown, L. E. Kidder, A. H. Mroue, H. P. Pfeiffer, M. A. Scheel, G. B. Cook, and S. A. Teukolsky, Phys. Rev. D **76**, 124038 (2007).
[50] M. Boyle, A. Buonanno, L. E. Kidder, A. H. Mroué, Y. Pan, H. P. Pfeiffer, and M. A. Scheel, Phys. Rev. D **78**, 104020 (2008).
[51] P. Grandclément, Phys. Rev. D **74**, 124002 (2006); **75**, 129903(E) (2007).
[52] K. Taniguchi, T. W. Baumgarte, J. A. Faber, and S. L. Shapiro, Phys. Rev. D **74**, 041502(R) (2006).
[53] K. Taniguchi, T. W. Baumgarte, J. A. Faber, and S. L. Shapiro, Phys. Rev. D **75**, 084005 (2007).
[54] K. Taniguchi, T. W. Baumgarte, J. A. Faber, and S. L. Shapiro, Phys. Rev. D **77**, 044003 (2008).
[55] F. Foucart, L. E. Kidder, H. P. Pfeiffer, and S. A. Teukolsky, Phys. Rev. D **77**, 124051 (2008).
[56] M. Shibata and K. Uryū, Phys. Rev. D **74**, 121503(R) (2006).
[57] M. Shibata and K. Uryū, Classical Quantum Gravity **24**, S125 (2007).
[58] M. Shibata and K. Taniguchi, Phys. Rev. D **77**, 084015 (2008).
[59] Z. B. Etienne, J. A. Faber, Y. T. Liu, S. L. Shapiro, K. Taniguchi, and T. W. Baumgarte, Phys. Rev. D **77**, 084002 (2008).
[60] M. D. Duez, F. Foucart, L. E. Kidder, H. P. Pfeiffer, M. A. Scheel, and S. A. Teukolsky, Phys. Rev. D **78**, 104015 (2008).
[61] T. Yamamoto, M. Shibata, and K. Taniguchi, Phys. Rev. D **78**, 064054 (2008).
[62] Z. B. Etienne, Y. T. Liu, S. L. Shapiro, and T. W. Baumgarte, Phys. Rev. D **79**, 044024 (2009).
[63] M. Shibata, K. Kyutoku, T. Yamamoto, and K. Taniguchi, Phys. Rev. D **79**, 044030 (2009).
[64] S. Brandt and B. Brügmann, Phys. Rev. Lett. **78**, 3606 (1997).
[65] T. W. Baumgarte, Phys. Rev. D **62**, 024018 (2000).
[66] E. Berti, S. Iyer, and C. M. Will, Phys. Rev. D **77**, 024019 (2008).
[67] J. W. York, Phys. Rev. Lett. **82**, 1350 (1999).
[68] G. Cook, Living Rev. Relativity **5**, 1 (2000).
[69] J. R. Wilson and G. J. Mathews, Phys. Rev. Lett. **75**, 4161 (1995).
[70] R. Beig, Phys. Lett. **69A**, 153 (1978).
[71] A. Ashtekar and A. Magnon-Ashtekar, J. Math. Phys. (N.Y.) **20**, 793 (1979).
[72] P. C. Peters and J. Mathews, Phys. Rev. **131**, 435 (1963).
[73] P. C. Peters, Phys. Rev. **136**, B1224 (1964).
[74] C. S. Kochanek, Astrophys. J. **398**, 234 (1992).
[75] L. Bildsten and C. Cutler, Astrophys. J. **400**, 175 (1992).
[76] M. Shibata, Phys. Rev. D **58**, 024012 (1998).
[77] S. A. Teukolsky, Astrophys. J. **504**, 442 (1998).
[78] S. Bonazzola, E. Gourgoulhon, and J.-A. Marck, Phys. Rev. D **56**, 7740 (1997).
[79] E. Gourgoulhon, P. Grandclément, K. Taniguchi, J.-A. Marck, and S. Bonazzola, Phys. Rev. D **63**, 064029 (2001).
[80] L. M. Lin and J. Novak, Classical Quantum Gravity **24**, 2665 (2007).
[81] L. Blanchet, Phys. Rev. D **65**, 124009 (2002).
[82] L. Blanchet, Living Rev. Relativity **9**, 4 (2006).
[83] LORENE website, http://www.lorene.obspm.fr/.
[84] G. B. Cook and H. P. Pfeiffer, Phys. Rev. D **70**, 104016 (2004).
[85] M. Caudill, G. B. Cook, J. D. Grigsby, and H. P. Pfeiffer, Phys. Rev. D **74**, 064011 (2006).
[86] G. B. Cook and B. F. Whiting, Phys. Rev. D **76**, 041501(R) (2007).
[87] D. Lai, F. A. Rasio, and S. L. Shapiro, Astrophys. J. Suppl. Ser. **88**, 205 (1993).